17th World Conference on Earthquake Engineering, 17WCEE
Sendai, Japan - September 13th to 18th 2020

SHALLOW STRUCTURE OF THE TANGSHAN FAULT ZONE FROM CONVERTED WAVES AND MICROTREMOR WITH A DENSE ARRAY

F. Bao[(1)], Z. Li[(2)]

[(1)] *Associate researcher, State Key Laboratory of Geodesy and Earth's Dynamics, Institute of Geodesy and Geophysics, Chinese Academy of Sciences, baofeng@whigg.ac.cn*
[(2)] *Professor, State Key Laboratory of Geodesy and Earth's Dynamics, Institute of Geodesy and Geophysics, Chinese Academy of Sciences, zwli@whigg.ac.cn*

Abstract

Reliable knowledge of sedimentary thicknesses is beneficial for investigating buried active faults and improving seismic hazard assessments, especially in regions with recent strong earthquakes. The Tangshan fault zone is regarded to be the seismogenic fault responsible for the 1976 Ms7.8 Tangshan earthquake, North China, which caused more than 240,000 deaths and became one of the most devastating earthquakes in the last 100 years in the world. From January to March 2017, a dense seismic array (comprising 152 seismographs with inter-station distances of approximately 1 ~ 4 km) was deployed in the Tangshan fault zone. More than 100 local events of magnitude 0 to 2 were recorded by the dense seismic array in the region. The larger tens of these events were located with NonLinLoc program and the horizontal components were rotated to radial and tangential. Three-component digital seismograms of these events are characterized by (1) the very weak direct S arrivals on the vertical component, which can be identified clearly from the one or two horizontal components, and (2) generally at least two prominent secondary arrivals between the direct P and S arrivals, one (Sp) dominant on the vertical component and another (Ps) with smaller amplitude on the two horizontal components. Travel-time differences between the Sp and S and between the P and Ps are the same for different events recorded at the same station but are different at different stations even for the same earthquake. These two secondary arrivals are the P-to-S (Ps) and S-to-P (Sp) converted waves that occur at the basement of the sedimentary basin beneath each station. We also investigate the sedimentary basement with the microtremor horizontal-to-vertical spectral ratio (H/V) method. For the ambient vibration survey, we obtain the resonance frequency from most seismographs, implying the sediment thickness. Based on the relations between resonance frequency and sediment thickness from borehole records, we also recover the sediment thickness around the Tangshan fault zone, compared with converted waves' results. Our results are also generally consistent with those of previous drilling and geological studies. Variations in the thickness of sediments indicate that the subsurface structure of the Tangshan fault zone has experienced significant modifications in its configuration, partially due to predominant tectonic control by the NE-SW trending Tangshan Fault Belt. The obtained sedimentary thicknesses provide an important model for earthquake strong motion simulations, sediment crustal corrections for travel time tomography and active fault investigations in the Tangshan fault zone.

Keywords: dense seismic array; local earthquake converted wave; Sp phase; H/V spectral ratio; Tangshan fault zone

1. Introduction

The Tangshan Fault is regarded as the seismogenic fault responsible for the 1976 Ms7.8 Tangshan earthquake, North China, one of the most devastating earthquakes to occur worldwide in the last 100 years. The Tangshan great earthquake is a rare intraplate event that has not yet been thoroughly investigated. Many moderate and small earthquakes have occurred throughout the earthquake region in recent years (Fig. 1). The bedrock underlying the Tangshan earthquake region was uplifted during the Mesozoic and early Cenozoic; as a result, sediments hundreds of meters thick cover nearly the entire region (Fig. 1a). The active faults throughout the Tangshan earthquake region are covered by Quaternary sediments with a thickness reaching close to 1 km. Consequently, it is imperative to detect the sediment structures and active faults around the Tangshan area at a high resolution to evaluate the corresponding earthquake hazard and improve the regional disaster prevention capabilities.

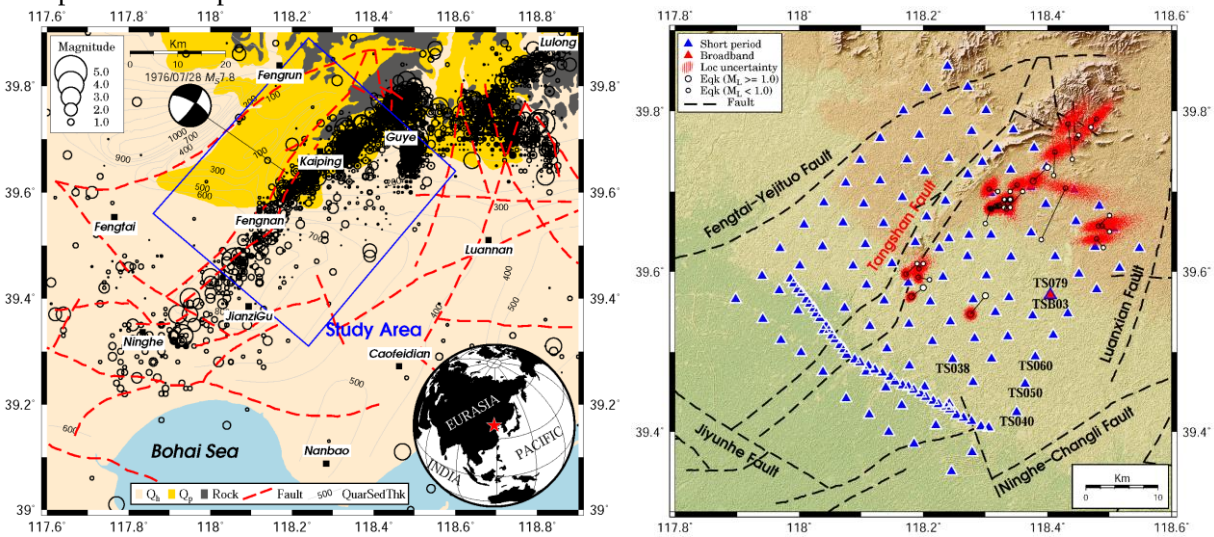

Fig. 1 – (a) Seismicity in the Tangshan earthquake region, including all moderate and small events (open circles, from 2010 to 2019 and the regional Quaternary geological map, in which gray blocks represent bedrock, orange blocks represent Pleistocene deposits (Qp), and khaki blocks represent Holocene deposits (Qh). The gray lines and numbers represent Quaternary isopachs and the thicknesses of Quaternary deposits, respectively, based on sparse geological drillings. The focal mechanism of the 1976 Ms7.8 Tangshan earthquake is also provided, and the red dashed lines provide details about the major faults [7]. (b) Dense seismic array (blue triangles) throughout the Tangshan earthquake region and epicentral locations of local small and micro earthquakes (circles) from 1 January to 31 March 2017. The posterior probability density function of the earthquake relocation is represented by the red point cloud, and the maximum likelihood solution is shown as an open circle [7].

In recent years, seismic methods have been developed to image the shallow and deep crust based on passive sources that provide numerous benefits, such as a low cost, a high efficiency, and a considerable efficacy. They have been applied to image the crustal velocity structure along active faults [1], to survey basins [2], and to explore for geothermal resources. These methods can be classified as seismic array and single-station methods. The seismic array method is based mainly on waveform cross-correlations and spatial autocorrelations to extract the dispersion curves of surface waves and then image the shear-wave velocity (Vs) structure [3]. In contrast, the single-station method is based on three-component microtremor or event waveform recordings to invert the shallow sediment structure for the fields of interest in engineering geological investigations.

The main objective of this study is to propose two passive seismic method to infer the variations in the thickness of unconsolidated Quaternary alluvial sediments for the development and construction of infrastructure.

2. H/V spectral ratio method

The reliability of H/V method has been verified in detecting the impedance contrast between loose deposits and seismic bedrock [4]. The microtremor wavefield measured by a three-component seismometer and the calculation of the ratio between its horizontal and vertical Fourier spectra are required in this method. The peak frequency in the H/V curve represents the fundamental resonance frequency that can be associated with the depth of the main seismic impedance contrast and the average shear-wave velocity above the contrast interface.

Assume that the subsurface velocity structure model is composed of a stack of homogeneous and isotropic horizontal layers overlying a homogeneous half-space. The observed resonance frequencies (f_r) of the sedimentary layers are linked to their thicknesses h (i.e., depths to seismic bedrock) and average shear-wave velocity V¯_S through the following formula:

$$f_r = \frac{\bar{V}_S}{4h} \tag{1}$$

The operating length usually ranges from 30 minutes to several hours to obtain a robust estimate of the microtremor wavefield characteristics. The processing of the individual measurement recordings generally includes windowing of short duration, selection of time windows to exclude strong transients and smoothing of the calculated amplitude spectrum [5].

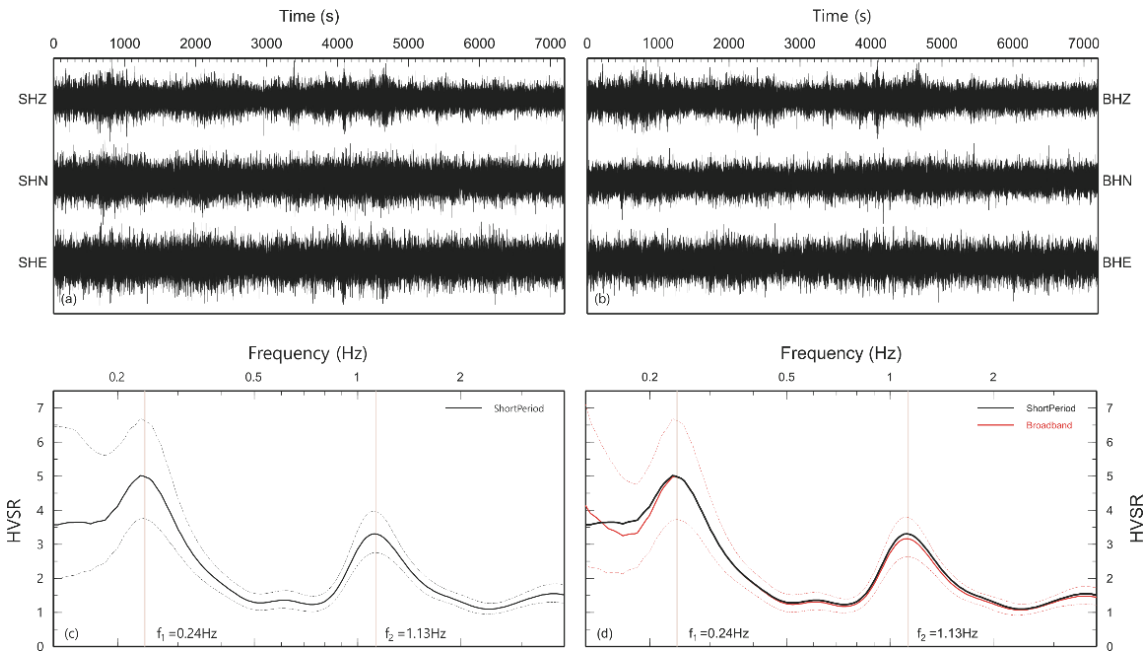

Fig. 2 – Comparisons and verifications of the H/V curves from short-period and broadband seismometers [1].

3. Local S-Sp or Ps-P method

To analyze the variations in the travel time with the sediment thickness, we use the F-K method to compute synthetic seismograms at a focal depth of 15 km (the mean depth in North China) with an epicentral distance of 20 km (according to the aperture of the Tangshan dense seismic array); the sediment thickness ranges from 0.05 to 1.00 km with an increment of 0.05 km. The three-component synthetic waveforms sorted by the sediment thickness and aligned in time by the direct S-wave arrival time are shown in Fig. 3.

The synthetic waveforms show the following. (1) Direct P waves are clear on the vertical component, while direct S waves are clear on the tangential component. (2) On the vertical component, there is a phase between the direct P and S waves with a stronger amplitude than the former, and the arrival time is identical

to the theoretical arrival time of the Sp wave. (3) There is another phase between the P and S waves on the radial component, and the arrival time is identical to the theoretical arrival time of the Ps wave. (4) The value of $dt_{(S-Sp)}$ is almost linearly correlated with the sediment thickness. (5) The value of $dt_{(Ps-P)}$ increases with the sediment thickness. (6) The value of $dt_{(S-Sp)}$ is similar to that of $dt_{(Ps-P)}$ at the same station in the same thickness model.

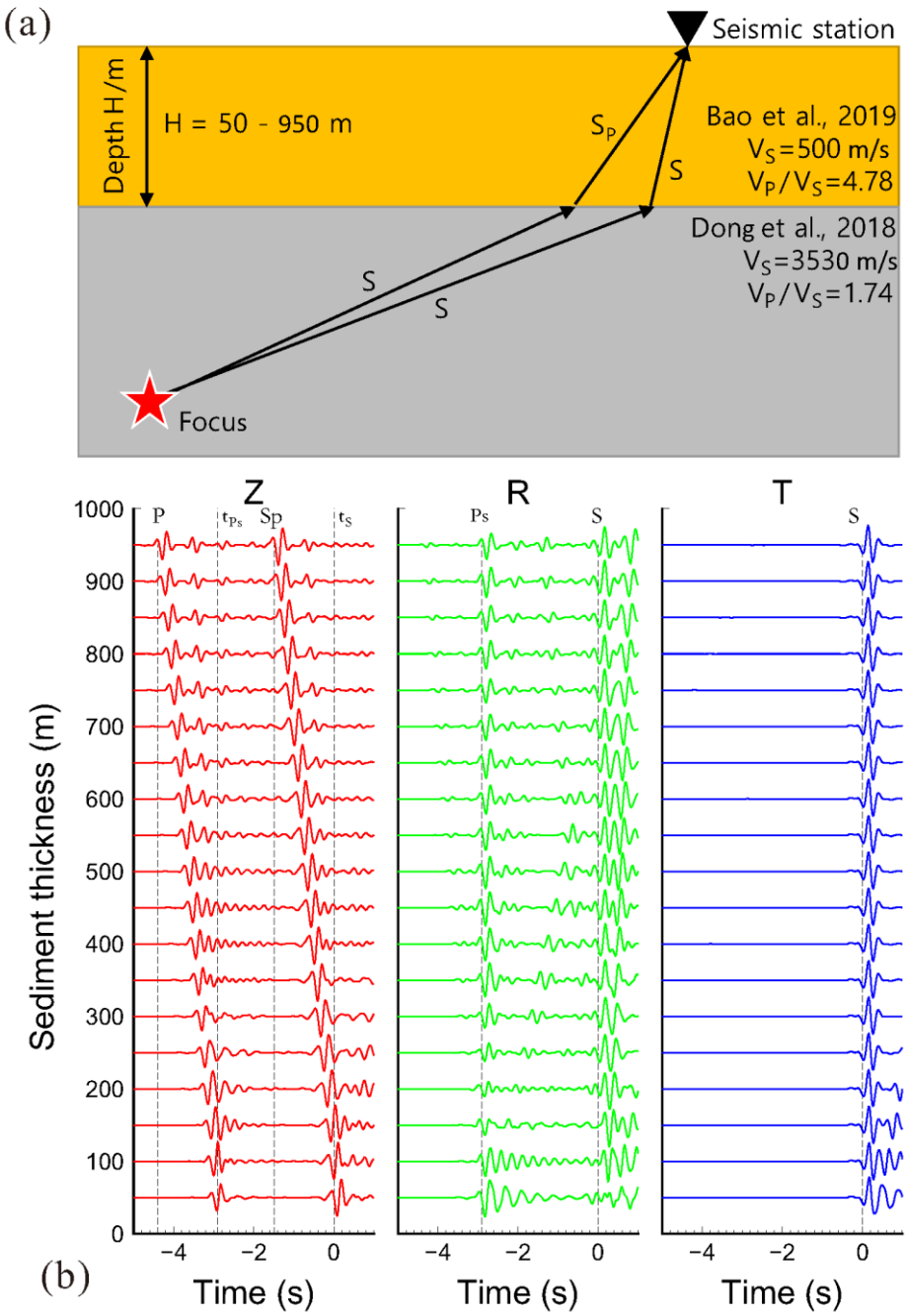

Fig.3 – Synthetic seismogram simulation. (a) Sedimentary model for the synthetic waveform simulation. Ray paths of direct S and local Sp converted waves. The inverted triangle indicates the seismic station [7]. (b) Three-component synthetic seismogram variation with the sediment thickness and the forward-modeled phases of direct P and S waves and of Sp and Ps converted waves [7].

Assume that the seismic waves arrive at the stations on the surface at an almost vertical angle of incidence due to a large velocity contrast across the boundary between the extremely low-velocity sediments and the underlying rocks. Thus, the travel-time difference between the direct and converted phases at a surface station situated atop sediment can be expressed as

$$dt_{(S-S_P)} = dt_{(P_S-P)} = \frac{H}{\bar{V}_S} - \frac{H}{\bar{V}_P} \tag{2}$$

where $dt_{(S-S_P)}$ is the difference in the travel time (in seconds) between the S and Sp phases, $dt_{(P_S-P)}$ is the difference in the travel time (in seconds) between the Ps and P phases, H is the sediment thickness (in km) beneath the station, and $\bar{V}_P$ and $\bar{V}_S$ are the average P- and S-wave velocities (in km/s) of the sediment, respectively. $dt_{(S-S_P)}$ is sensitive primarily to the thickness and average Vs of the sedimentary cover.

In the above equation, both $\bar{V}_S$ and $\bar{V}_P$ are known, and either $dt_{(S-S_P)}$ or $dt_{(P_S-P)}$ is measured for different stations; Therefore, the thickness H of the sediments overlying the bedrock can be approximated as

$$H = \frac{\bar{V}_S \times dt_{(S-S_P)}}{1-\bar{V}_S/\bar{V}_P} = \frac{\bar{V}_S \times dt_{(P_S-P)}}{1-\bar{V}_S/\bar{V}_P} \tag{3}$$

To accurately identify the arrival times of the Sp converted phases and direct S phases, we first relocate all the selected events with the data from the dense seismic array. Then, we rotate the two horizontal components into radial and tangential orientations to better identify the direct S-wave arrivals. Additionally, we identify the P- and Sp-wave arrivals on the vertical component. A total of 25 events recorded by 80 stations throughout the Tangshan earthquake region are utilized, resulting in 359 manually picked travel-time differences of S-Sp arrivals. After measuring $dt_{(S-S_P)}$, we calculate the sediment thickness according to Eq. (3).

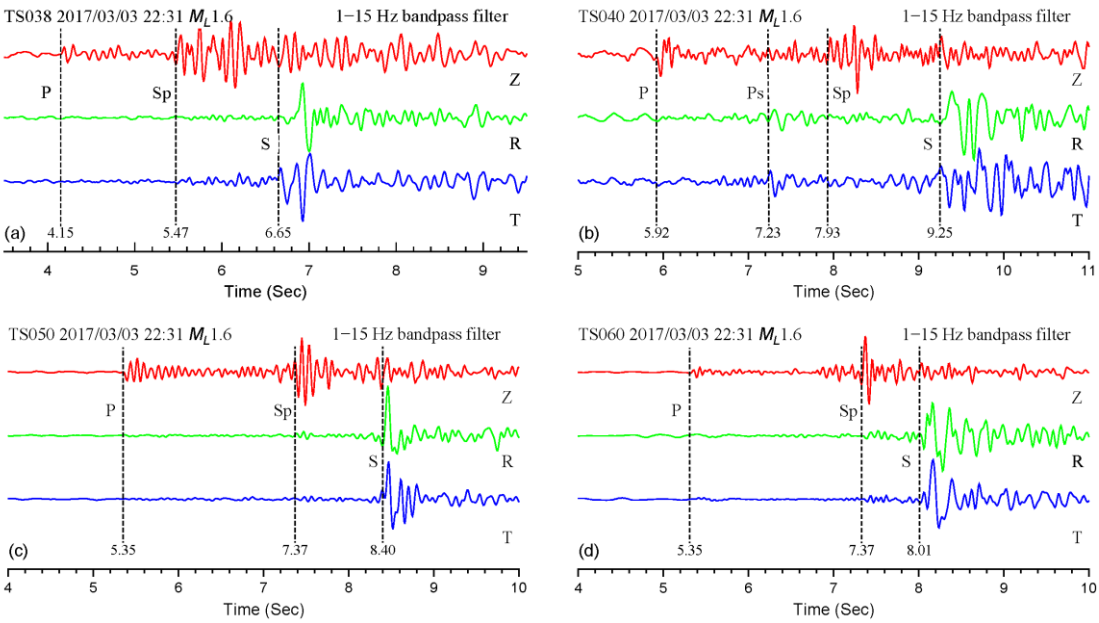

Fig. 4 – Three typical examples of local Sp converted phases and Ps converted phases recorded by the Tangshan dense seismic array. The direct P and S phases and Sp and Ps converted phases are marked at each station (see Fig. 1b) [7].

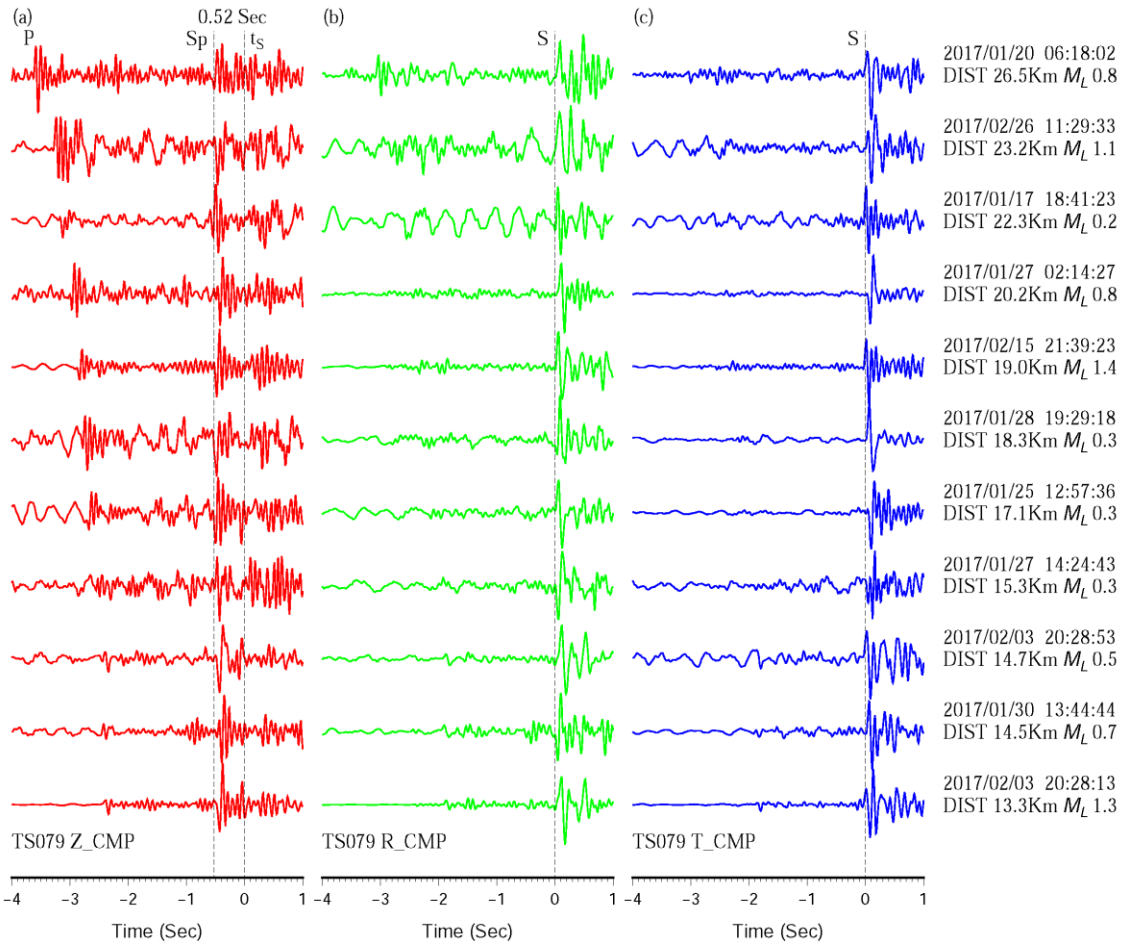

Fig. 5 – Three-component waveforms from station TS079 (see Fig. 1b) for different events sorted by their epicentral distances and aligned in time by the direct S-wave arrival times [7].

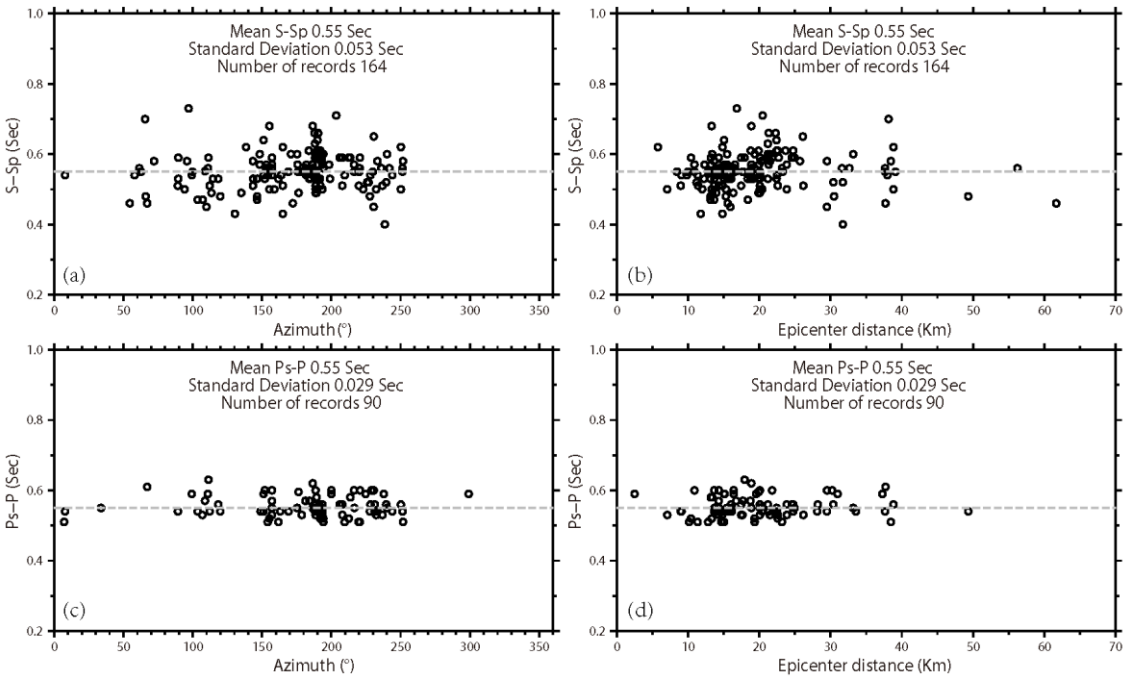

Fig. 6 – Travel-time differences between the direct and converted waves for different earthquakes from January 2017 to March 2019 located at different azimuths and epicentral distances but recorded at the same broadband station (TSB03). It is clear that the values of $dt_{(S-S_P)}$, the same as those of $dt_{(P_S-P)}$, are constant at station TSB03 regardless of the earthquake locations [7].

4. H/V measurements with TSarray

To explore the variations in the resonance frequencies, which are defined as the lowest frequencies of spectral peaks from the computed H/V curves, in relation to the basement structure, we prepare a resonance frequency map for the study area by gridding the resonance frequency values over the measurement points (Fig. 7a).

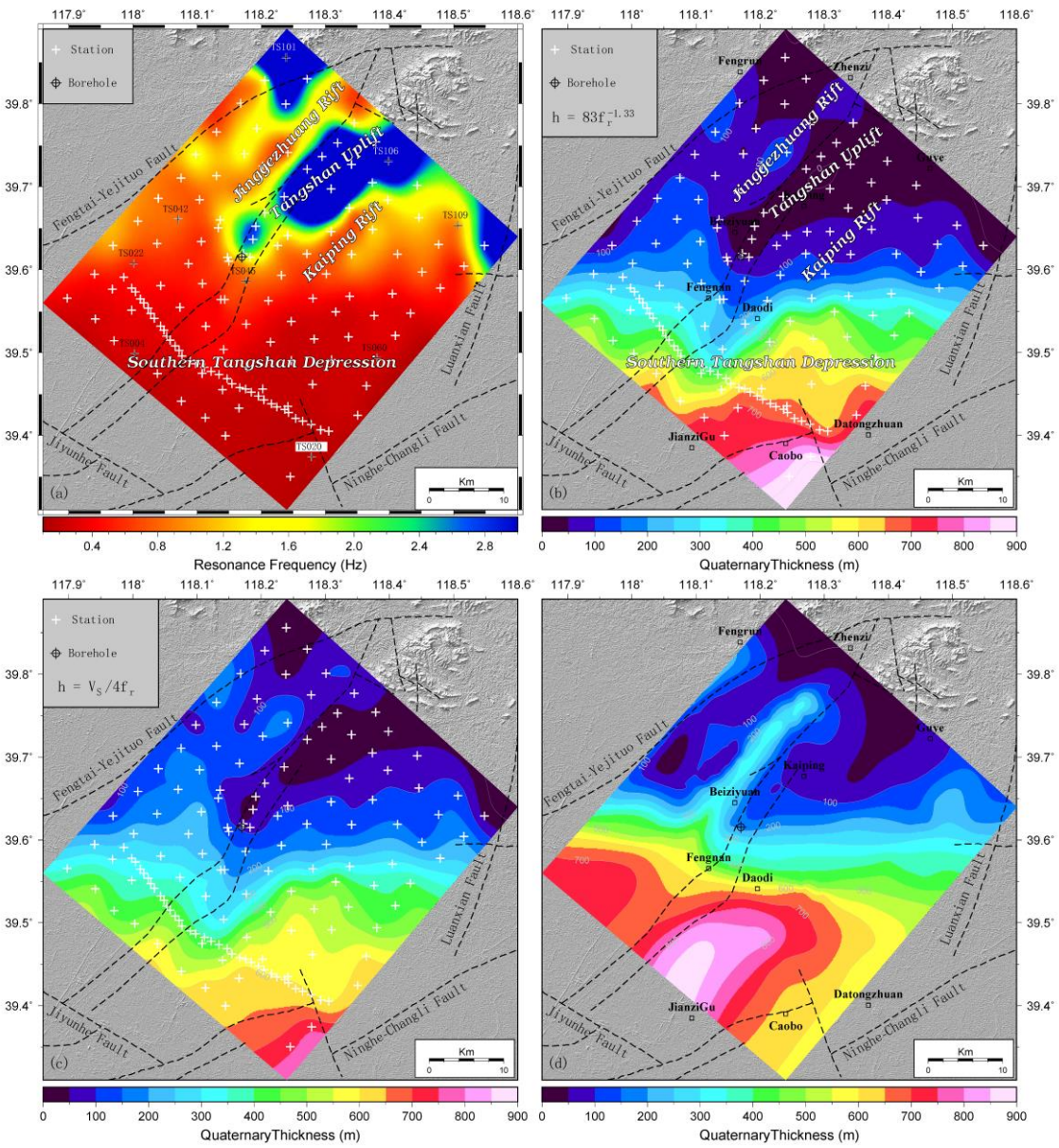

Fig. 7 – (a) Resonance frequency (in Hz) distribution with H/V microtremor survey sites (white crosses) and (b, c, and d) Quaternary thicknesses (in metres) around the Tangshan fault zone [2]. Panels (b) and (c) are maps showing the thickness of the sedimentary infill derived from the H/V resonance frequency by different

frequency-thickness relationships (see upper left label of each panel). (d) Contour map showing the thickness of the Quaternary sediment from sparse geological drillings [2].

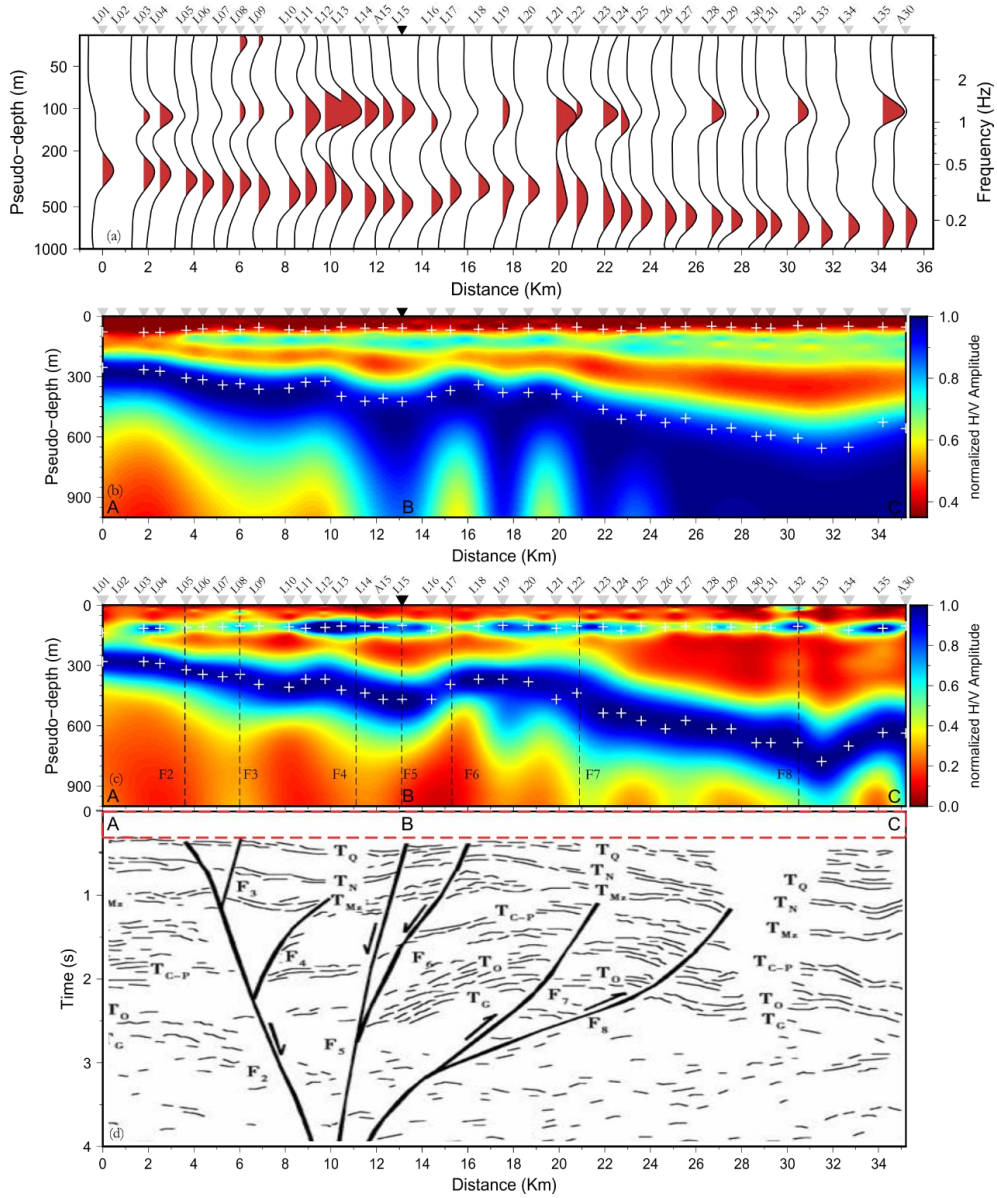

Fig. 8 – (a) The calculated H/V curve profile; (b) The theoretical H/V pseudo-depth profile [1]; (c, d) Comparing calculated pseudo-depth profile with deep seismic reflection profiling (modified from [4]). F1-F8 represent the conjectural faults. T_Q is Quaternary sedimentary basement, T_N is the substratum of Neogene. T_{Mz} is Mesozoic crystalline basement, T_O and $T_{C\text{-}P}$ are the interfaces of Paleozoic Ordovician and Carboniferous-Permian strata. T_C is the interface between upper and lower crust, and T_M represents crust-mantle transitional zone [1].

By analysing the H/V curves, we find that the predominant resonance frequency has a range of 0.15 - 3 Hz in most parts of the Tangshan fault zone. Referring to the average shear-wave velocity of 250-500 m/s [1], the sediment thickness in most regions has a range of 20-850 m as predicted by eq. (1). We observe a maximum thickness of ~ 900 m in the southern Tangshan depression, and the thickness varies in accordance with the topography and surface geology, reaching close to zero where the bedrock crops out.

Sediment thickness distributions are calculated for the study area based on our derived power-law equation [2] in Fig. 7b and the inverse proportion equation in Fig. 7c. The sediment thickness map for the study area is also compiled based on sparse geological drillings in Fig. 7d. The H/V-derived sediment thickness presented in this study generally coincides with the results of previous geological surveys in the whole region. For example, the sediment is much thinner on the northern side and much thicker on the southern side of the study area. Moreover, the new sediment thickness maps provide more details with much smaller undulations over the entire area than those in previous studies. These small-scale fluctuations appear to be reasonably consistent with the surface morphology and subsurface geology in this area. A comparison of the H/V-derived thicknesses and the drilling survey reveals some inconsistencies, especially in the deepest depocentre location. A dense calibration seismic profile was conducted across the entire disputed region of the southern study area with an inter-station distance of ~ 1 km perpendicular to the Tangshan Fault, and it revealed two significant seismic impedance interfaces at depths of ~ 100 m and 300-800 m. Related research results have verified good consistency with the seismic reflection interfaces from shallow seismic reflection exploration and deep seismic reflection profiling (Fig. 8).

5. Local S-Sp measurements with TSarray

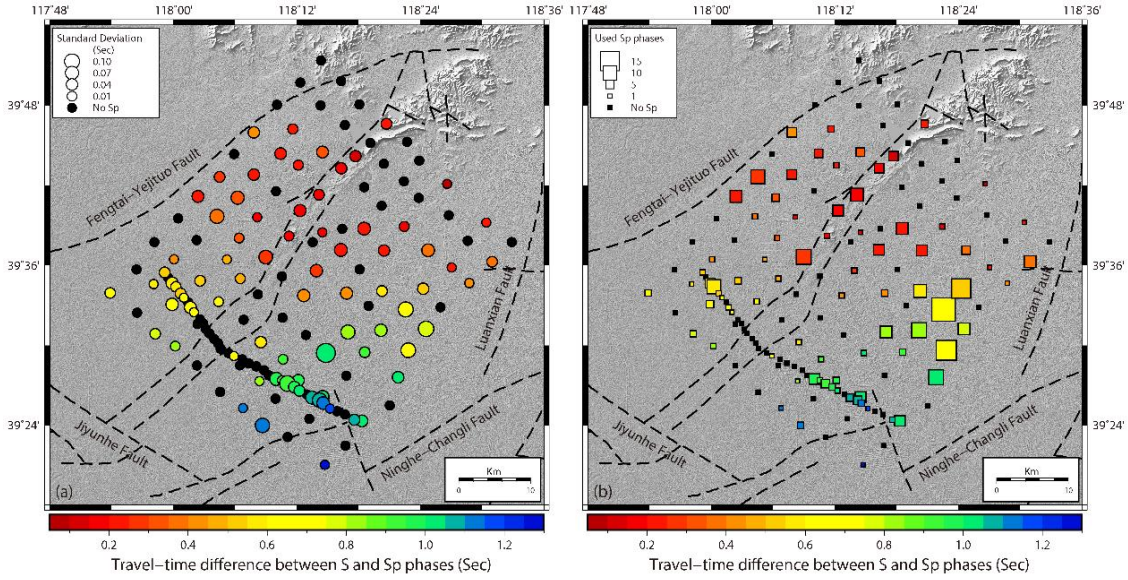

Fig. 9 – Spatial distribution of the measured mean $dt_{(S-S_P)}$, including the corresponding standard deviation and the number of Sp phases used at each station [7].

We manually pick the S- and Sp-phase arrival times from the three-component seismic waveforms recorded during 25 events at 80 stations. The spatial distribution of the resulting S-Sp travel-time differences is plotted in Fig. 9. Small values of $dt_{(S-S_P)}$ (close to 0.2 s or smaller) are tightly concentrated in the vicinity of the north-central Tangshan earthquake region, which is characterized by a series of hills. The bedrock outcrops in these hills, corresponding geologically to the Tangshan Uplift and the southern margin of the Yanshan Uplift. Sp phases are not observed at the edge of this area where bedrock outcrops are concentrated, which is also near a densely populated downtown district. However, large $dt_{(S-S_P)}$ values (0.6-1.2 s) are distributed in the southern region. The maximum $dt_{(S-S_P)}$ of 1.26 s is observed in the Caobo region in the southern part of the study area, within the depression near the Ninghe-Changli Fault. The values of $dt_{(S-S_P)}$ are more or less constant beneath each station with a small standard deviation mostly less than 0.1 s. The stations with the most Sp observations are located in the eastern part of the study area, while the stations that recorded the

fewest Sp observations are located in the northern region of outcropping bedrock, the downtown district of Tangshan and the region adjacent to the Tangshan Fault.

6. Uncertainty in the thickness differences between the local Sp and H/V methods

The sediment thickness beneath each station is calculated based on the local S-Sp method. The thicknesses beneath all 80 stations are predicted by Eq. (3). A map of the sediment thickness for the whole study area is produced by linearly interpolating the sediment thicknesses from nearby stations (Fig. 10a).The thickness of the Quaternary sediments in most of the study region ranges from 50 to 800 m and becomes thicker toward the south; in other words, the sediment is much thinner on the northern side and much thicker on the southern side of the study area. The towns of Fengnan and Daodi are located along the dividing boundary of a thickness variation and near the Tangshan Fault, respectively. We observe a maximum thickness of ~ 800 m in the southern Tangshan depression. These small-scale fluctuations appear to be reasonably consistent with the topography and subsurface geology in this area, and the sediment thickness approaches zero where the bedrock outcrops in the northern region.

To justify the spatial distribution of sediment structure beneath Tangshan fault zone, we compare the local S-Sp measurements with the thicknesses of Quaternary sediments in the same study area obtained by microtremor H/V surveys, as shown in Fig. 10b. The thickness of the Quaternary sediments derived from the H/V method varies from 20 to 800 m in most areas, which is consistent with the results of the local S-Sp method. We display the differences in the sediment thicknesses estimated between the local S-Sp method and the H/V surveying approach in Fig. 10b, which shows that at most stations, the difference in the measurements between these two methods is less than 60 m. The maximum difference reaches 97 m at station TS007. Therefore, a station that is situated to better observe the arrivals of converted waves, such as a station in the central-eastern region of the study area, can be used to obtain a more reliable sediment thickness.

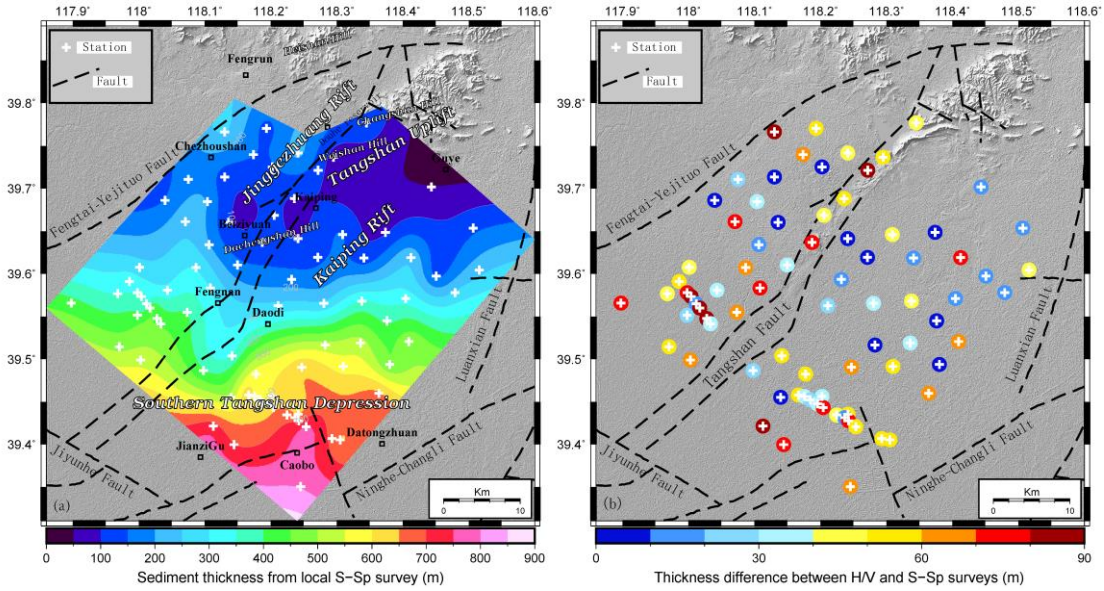

Fig. 10 – (a) Sediment thickness based on the local S-Sp method and the main geological tectonic units in the Tangshan earthquake region [7]. (b) Thickness differences between the measurements based on the local S-Sp method and the microtremor H/V surveying approach in the Tangshan earthquake region [7].

7. Conclusions

We develop a microtremor horizontal-to-vertical spectral ratio (H/V) method based on ambient seismic data from a dense seismic array to clearly reveal two seismic impedance interfaces at depths of ~ 100 m and 300 ~ 800 m by examining two-dimensional H/V profiles crossing the Tangshan Fault. Furthermore, the same method was successfully employed to demonstrate that the thickness of the Quaternary sediments varies from less than 200 m in the northern Tangshan earthquake region to ~ 800 m in the south. In addition, by effectively utilizing the travel-time differences between direct S waves and Sp converted waves generated by local small and micro earthquakes, the shallow sediment structure in the study area is also obtained. The variation in the thickness derived from the local S-Sp method is consistent with the thickness of sediments imaged from microtremor H/V surveys. Hence, the proposed approach provides an independent way to determine the thickness of Quaternary sediments in an urban area. The findings of these studies are generally consistent with those of previous drilling and geological investigations, all of which indicate that the Tangshan Fault has been significantly ruptured and modified by strong earthquake activities since the Quaternary.

This work delineates the relationship between the fault system and the sediment thickness and thus is of great significance for investigating active faults and simulating earthquake strong motions. Several identified buried tectonic structures are compatible with the fault arrangement recognized at the surface. The variations in sediment thickness reflect a complex subsurface architecture in the Tangshan earthquake region, which is characterized by topographic highs and lows that represent tectonic uplifts and depositional districts, respectively. The main depositional district is recognized to the south of the Tangshan earthquake region, which is characterized by distinctively different infill thicknesses. This result implies that the maximum sediment thickness is in the southern Tangshan earthquake region near the Ninghe-Changli Fault. The subsurface model highlights that the Tangshan earthquake region has experienced considerable transformations in its architecture over time, and its overall geometry reveals tectonic control by faults that are part of the NNE-striking extensional Tangshan Fault.

8. Acknowledgements

The authors are grateful to the staff of the Tangshan Central Seismic Station of the Earthquake Administration of Hebei Province for their support with the seismic observations. This work was supported by grants 2018YFC1504202, NSFC41974064, NSFC41674065, NSFC41404052 and NSFC41874069. The study was also supported by the China Earthquake Science Experiment Project, China Earthquake Administration (2019CSES0102), and the State Key Laboratory of Geodesy and Earth's Dynamics.

9. Copyrights

10. References

[1] Bao F, Li Z, Yuen D, Zhao J, Ren J, Tian B (2018): Shallow structure of the Tangshan fault zone unveiled by dense seismic array and horizontal-to-vertical spectral ratio method. *Physics of the Earth and Planetary Interiors*, **281**, 46-54.

[2] Bao F, Li Z, Tian B, Wang L, Tu G (2019): Sediment thickness variations of the Tangshan fault zone in North China from a dense seismic array and microtremor survey. *Journal of Asian Earth Sciences*, **185**, online.

[3] Li Z, Ni S, Zhang B, Bao F, Zhang S, Deng Y, Yuen D (2016): Shallow magma chamber under the Wudalianchi volcanic field unveiled by seismic imaging with dense array. *Geophysical Research Letters*, **43**(10), 4954-4961.

[4] Nakamura Y (1989): A method for dynamic characteristics estimations of subsurface using microtremors on the ground surface. *Quarterly Report of Railway Technical Research Institute*, **30**(1), 25-33.

[5] Konno K, Ohmachi T (1998): Ground-motion characteristics estimated from spectral ratio between horizontal and vertical components of microtremor. *Bulletin of Seismological Society of America*, **88**(1), 228-241.

[6] Liu B, Qu G, Sun M, Liu K, Zhao C, Xu X, Feng S, Kou K (2011) Crustal structures and tectonics of Tangshan earthquake area: Results from deep seismic reflection profiling. *Seismology and Geology*, **33**(4), 901-912.

[7] Bao F, Li Z, Shi Y, Tian B, Wang H (2020): Sediment structures constrained by Sp waves from local earthquakes recorded by a dense seismic array in the Tangshan earthquake region. *Geophysical Journal International*, under review.

